Investigation of particle shape and size effects in SERS using *T*-matrix calculations

Rufus Boyack and Eric C. Le Ru*

Received 20th March 2009, Accepted 6th May 2009
First published as an Advance Article on the web 9th June 2009
DOI: 10.1039/b905645a

The influence of particle size and shape effects on average and punctual surface-enhanced Raman scattering (SERS) enhancement factors (EFs) is investigated using exact *T*-matrix electrodynamic calculations of silver and gold spheroids over a large parameter space. This study extends the conventional treatment of these effects within the frameworks of the electrostatics approximation, its generalizations, or Mie theory for spheres. It confirms the qualitative features of these approaches, but provides in addition quantitative predictions of SERS EFs in the case of large non-spherical particles, where the lightning-rod effect (shape effect) and radiation damping (size effect) operate simultaneously. Finally, the localization effect at large SERS EF (hot-spots) is shown to be dictated only by shape, not size, in the case of metallic spheroids at the dipolar localized surface plasmon resonance.

I. Introduction

Surface-enhanced Raman spectroscopy[1,2] (SERS) is increasingly used as a tool in a variety of applications, ranging from ultra-sensitive chemical analysis[3] to bio-sensing.[4,5] For this trend to continue and expand further, it is desirable to devise and fabricate robust SERS substrates with adequate properties, including but not limited to: (i) ease of fabrication and low-cost, (ii) reproducibility and uniformity, (iii) re-usability (or even disposable if low-cost), (iv) surface-functionalization if a particular analyte is targeted, (v) suitable (*i.e.* large) SERS enhancements.

The latter point is crucial, but its meaning may vary depending on the application. A large *average* enhancement factor (EF) is typically required for most sensing/analytical applications. However, only a large *maximum* EF is needed for single-molecule detection,[6–8] and it may be highly localized in specific regions on the surface, so-called SERS hot-spots.[9] For this reason, a large maximum EF may not *a priori* be equivalent to a large average EF. In addition, since large enhancements are intrinsically linked to underlying localized surface plasmon (LSP) resonances of the substrate, any SERS substrate is typically only optimized to work in a specific wavelength range, and possibly only for a given incident electric polarization.

In order to meet these challenges, a good theoretical understanding of the factors affecting the average and maximum SERS EF is desirable. These include (i) composition, *i.e.* intrinsic optical properties of the materials, (ii) size, (iii) shape, (iv) interactions and gap effects for multiple particles (v) effects of composite structures (such as nano-shells[10,11]). We focus in this paper on the shape effect, for gold and silver nanoparticles. To this end, we consider the spheroid model (for both oblate and prolate spheroids) and solve *exactly* the electromagnetic problem in a variety of cases. This study therefore complements and extends the classical description of shape effects in SERS in terms of the spheroid (*i.e.* ellipsoid of revolution) in the electrostatics approximation[1,12–14] and that of size effects in terms of the exact EM solution for a sphere[15,16] (Mie theory).

The "shape effect" in SERS has been recognized early on as a possible additional source of electromagnetic (EM) enhancement.[12] It manifests itself as two concomitant phenomena:[1] (i) firstly, a shift of the localized surface plasmon resonances (which are ultimately responsible for the SERS EM enhancement); (ii) secondly, a modification of the local field enhancements on the particle surface, compared to that obtained on a sphere. In situations of interest to SERS, the enhancement can indeed be magnified at the "tip" of elongated metallic nano-particles, when the excitation is polarized along this long axis (the resonance is then typically redshifted). This tip or corner effect is often called the "lightning rod effect" by analogy with the phenomenon occurring in the electrostatics theory of perfect conductors. Most of this phenomenology is well described by the EM model of SERS. It has so far mostly been studied within the relatively simple framework of metallic spheroids in the electrostatics approximation (ESA), which qualitatively accounts for the aforementioned effects. However, such an approximation is strictly only valid in the limit of ultra-small particles, typically for maximum dimensions less than $\lambda/20$, *i.e.* of the order of 20 nm in cases of interest to SERS. Beyond this size, retardation and radiation effects that cannot be modeled in the ESA begin to play an increasingly important role. These have been studied in simple cases like a sphere,[15,16] where the exact EM solutions can be obtained with Mie theory, confirming the limitations of the ESA.[1] These are particularly pronounced for low-absorbing metals like silver in the visible/infrared, or gold in the red/infrared and may affect dramatically the theoretical predictions of SERS enhancement

School of Chemical and Physical Sciences, Victoria University of Wellington, P.O. Box 600, Wellington 6143, New Zealand. E-mail: boyackrufu@student.vuw.ac.nz, Eric.LeRu@vuw.ac.nz

factors (EFs). A simple phenomenological description of these effects, in terms of finite-size corrections to the dipolar polarizability, has been proposed.[13,17,18] These so-called dynamic depolarization and radiation damping corrections to the ESA predict qualitatively the two main effects of a size increase: (i) a red-shift and broadening of the dipolar LSP resonance, and (ii) a marked decrease in the local field enhancements. However, by comparing these predictions with the exact calculations presented here, it appears that these corrections are not quantitative: they fail to predict the correct resonance shifts and local field enhancements, even for relatively small sizes. Moreover, they ignore any higher order LSP resonances (*e.g.* quadrupolar), which may be important in some cases as we shall see.

Exact calculations are therefore desirable. They can be carried out numerically, for example using finite-element modeling,[19] finite-difference time-domain,[20] or boundary integral equation methods.[21] They however remain computationally intensive in the general case of a 3D particle, and their accuracy is difficult to assess *a priori* since it is very sensitive to the mesh finesse and bounding box size (when needed). Semi-analytic methods are therefore better suited to study a vast parameter space in terms of size and shape. The discrete dipole approximation[22,23] has for example been used extensively to predict light scattering properties by metallic particles of various shapes. However, its predictions in terms of local field at the surface are strongly limited by the finesse of discretization and cannot be trusted. The method of separation of variable can also be applied to spheroids[24,25] in a similar fashion as Mie theory for spheres. Although it has been applied successfully to model extinction/scattering spectra, it has not been used for local field predictions, probably because of its complexity.

A promising semi-analytic approach that circumvents many of these problems is the *T*-matrix or null-field method, also known as extended boundary condition method (EBCM).[26–30] It consists in expanding the EM fields in terms of vector spherical harmonics, as for Mie theory. The coefficients of these expansions can then be deduced from those of the incident field through the *T*-matrix. The *T*-matrix itself is computed from surface integrals on the particle under study, therefore eliminating any bounding box issues. The *T*-matrix has been used extensively for calculating far-field properties of dielectric particles of various shapes and of intermediate sizes (typically one to ten times the wavelength).[30–33] Its mathematical structure makes it particularly suited to calculations for small particles, for which convergence should be much faster. Despite these advantages, this has hardly been explored so far in the context of SERS and plasmonics[34] and in particular for local field calculations, except in the pioneering studies of Barber *et al.*[35,36] These demonstrated the feasibility and power of the *T*-matrix approach using a specific geometry: a prolate spheroid of aspect ratio 2 : 1.

We here extend this work to study the EM response and local field enhancements on the surface of both oblate and prolate spheroids with aspect ratios as large as 10 : 1. The EM problem and its practical solution are discussed in section II. We then present and discuss the results, focusing at first on the size and shape-induced shifts of the LSP resonances in section III. The SERS enhancements are then considered, focusing first on surface-averaged EF in section IV, and then on the points of highest enhancement (hot-spots) in section V.

II. Methods

The EM problem under study is shown schematically in Fig. 1. We consider an ellipsoid of revolution along axis z and centred at the origin O. c and a denote the z semi-axis and the x (and y) semi-axes, respectively. The aspect ratio is denoted h and is taken by convention as $h \geq 1$. We will distinguish two cases of interest: prolate spheroids ($c > a$, $h = c/a$) and oblate spheroids ($c < a$, $h = a/c$). Only excitation polarized along the long axis will be considered, since it is the most relevant to SERS. The excitation is chosen as a linearly polarized plane wave incident along a wave-vector $\boldsymbol{k}$. For the prolate spheroid, we therefore take $\boldsymbol{k}$ along x and the polarization along z (long-axis), a configuration called KxEz in the following. For the oblate spheroid, polarization is along x (one of the long-axis), but we need to consider two incident directions since the $\boldsymbol{k}$ vector breaks the symmetry: either along z (KzEx) or along y (KyEx). Note that these two would be equivalent in the electrostatics approximation. The size of the particle will be characterized by a single volume-equivalent radius $r_0 = (a^2c)^{1/3}$, *i.e.* the radius of a sphere of same volume. Its shape is then characterized simply by the aspect ratio h. The dimensions of the nanoparticles considered here are summarized in Table 1 for convenience.

We will study the optical response of such metallic nanoparticles composed of either silver or gold, the two most common metals for SERS. The wavelength-dependent dielectric function for both is obtained from the analytic expressions given in ref. 1 and 37. The embedding medium is chosen as water with dielectric constant $\varepsilon_M = 1.77$ in all cases. Similar conclusions would be obtained for other media.

All EM predictions are exact 3D electrodynamic calculations obtained using the *T*-matrix approach with the extended boundary condition method (EBCM).[28–30] *T*-matrix calculations have been carried out following the treatment

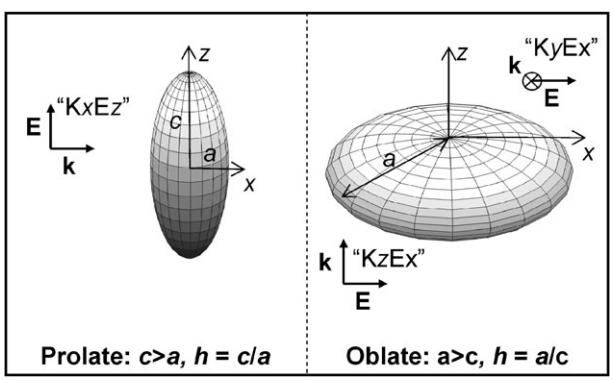

Fig. 1 Schematics of the two types of metallic nano-particles studied here: prolate and oblate spheroids with symmetry of revolution around the z axis. The incident excitations, characterized by a $\boldsymbol{k}$ vector and an electric (linear) polarization $\boldsymbol{E}$ are also shown (two for oblate, one for prolate because of symmetry). Note that the polarization is always taken along one of the long axis of the particle (this is the case where the highest enhancements are achieved).

Table 1 Geometrical properties of the oblate and prolate spheroid metallic particles considered in this study. a [nm] and c [nm] denote the semi-axis along x (same as y) and z, respectively. r_0 [nm] is the radius of a sphere of equal volume, *i.e.* $r_0^3 = a^2c$. The aspect ratio h is taken larger than 1 by convention, and we therefore have $h = a/c$ ($h = c/a$) for oblate (prolate) spheroids. All dimensions in the table are in nanometers and are rounded off (they are only provided to fix ideas, exact numbers may be calculated easily if needed)

	Oblate									
	2		3		5		8		10	
h	a	c	a	c	a	c	a	c	a	c
$r_0 = 10$	13	6.3	14	4.8	17	3	20	2.5	22	2.2
$r_0 = 30$	38	19	43	14	51	10	60	7.5	65	6.5
$r_0 = 50$	63	31	72	24	85	17	100	12	108	11
	Prolate									
	2		3		5		7			
h	a	c	a	c	a	c	a	c		
$r_0 = 10$	8	16	7	21	6	29	5	37		
$r_0 = 30$	24	48	21	62	18	88	16	110		
$r_0 = 50$	40	80	35	104	29	146	26	183		

given in ref. 30. We have used proprietary codes developed in Matlab with floating point calculations in double precision. The surface integrals required for the computation of the T-matrix were carried out using a Gauss quadrature with 300 points, for which satisfactory precision is obtained in all cases considered here (this can be easily checked by comparing the results with more or less integration points). An important point in all T-matrix calculations is to check convergence of the results,[30,38] *i.e.* determine the maximum indices n,m to include in the truncated series. Although it is customary to truncate both n and m indices,[38] we have included all $-n \leq m \leq n$ in our calculations. The n-series were truncated at $N_{\max}$ between 10 and 15, depending on the case. Convergence was checked by ensuring that both the predicted extinction cross-section and the average and punctual SERS EFs were not dependent on $N_{\max}$. This convergence test was only carried out in selected cases, typically those for which convergence is more challenging, *i.e.* largest aspect ratios. All local field calculations were carried out by evaluating the internal fields, *i.e.* the electric fields on the nano-particle surface, but *inside* the particle. Standard EM boundary conditions are then applied to deduce the surface field on the *outside* surface. This approach avoids having to rely on the (unproven) validity of the Rayleigh hypothesis.[30]

Once the surface fields are known, most EM and SERS properties, average or punctual can be derived. We will here focus on the local field intensity EF (LFIEF),[1] $M = |E|^2/|E_0|^2$, and the SERS EF at zero-Stokes shift in the $|E|^4$-approximation, $F = |E|^4/|E_0|^4$. The latter gives a simple yard-stick estimate of the expected SERS EF, with minor limitations that are well understood.[1,39] These EFs will be estimated at points of interest on the surface, in particular at the points along the incident polarization where the EFs are maximum at the dipolar LSP resonance. The surface-averaged SERS EFs, $\langle F \rangle$, will also be studied in detail since they are the most relevant in many applications. This differs slightly from earlier studies,[35,36] where only $\langle M \rangle$ was considered and $\langle F \rangle \approx \langle M \rangle^2$ was assumed. This latter expression is in fact not accurate and may underestimate $\langle F \rangle$ by a factor as large as 10 for large aspect ratios compared to the correct one: $\langle F \rangle = \langle M^2 \rangle$.

Finally, it is worth highlighting the fact that all calculations are carried out within the local approximation of the dielectric function (*i.e.* ε depends on ω but not on $\boldsymbol{q}$), or equivalently using abrupt metal/dielectric interfaces. Such an approach is standard in most SERS and plasmonics calculations, but it tends to overestimate the field enhancements at short distances from the metal surface (typically $d < 0.5$ nm[40]). Our predictions should therefore be viewed as upper estimates of the field EFs on the surface ($d = 0$ nm). Alternatively, since field enhancements in the local approximation do not vary much between $d = 0$ and $d = 1$ nm, our predictions can also be considered as the real field EFs at $d \approx 0.5$ nm, which is the typical distance for an adsorbed dye molecule.

III. Localized surface plasmon resonances

We first focus on the shape-induced redshifts of the LSP resonances and how they are affected by finite-size effects. These resonances appear clearly as peaks in the wavelength dependence of the far-field properties and we will therefore concentrate on these first. Fig. 2 shows the extinction spectra for a number of representative cases. It is plotted for convenience in terms of an adimensional extinction coefficient Q_{ext}, derived from the particle extinction cross-section σ_{ext} as: $Q_{\text{ext}} = \sigma_{\text{ext}}/(\pi r_0^2)$. A summary of the LSP resonance wavelengths for a wider range of parameters is also given in Fig. 3.

Some of the features evident in Fig. 2 and 3 are already predicted in the ES approximation: (i) a redshift of the resonance for higher aspect ratios; (ii) a larger redshift for prolate spheroids compared to oblate spheroids of same aspect ratio. Some aspects of the size-dependence are also similar to those predicted for a sphere using Mie theory, for example the redshift and broadening of the resonance as the size increases. There are in addition new aspects that could not be predicted within these approaches: (i) the aspect-ratio-induced and size-induced redshifts of the resonance are cumulative, resulting in fairly long resonance wavelength (even for Ag particles), close to 1.2 μm for example for a silver prolate spheroid with $r_0 = 50$ nm and $h = 5$. In fact the size-induced redshift is even more pronounced at larger aspect ratios. (ii) The broadening

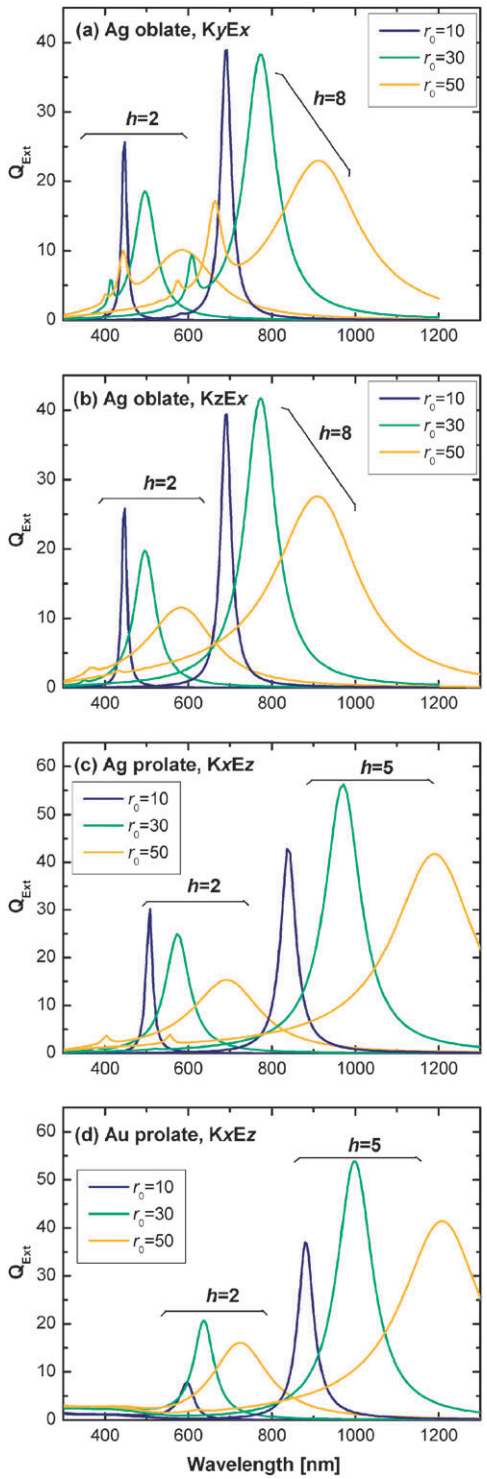

Fig. 2 Predicted spectral dependence of the extinction coefficient for a number of representative cases: Ag oblate spheroids of aspect ratio $h = 2$ and $h = 8$ for either (a) KyEx or (b) KzEx excitation, and (c) Ag or (d) Au prolate spheroids of aspect ratio $h = 2$ and $h = 5$ for KxEz excitation.

of the resonance does not appear to be much affected by aspect ratio, but only by size. The resonance broadening is comparable for a given size at two different aspect ratios, despite the large difference in resonance wavelength, *i.e.* redshift and broadening are no longer correlated when both shape and size effects are at present. (iii) For oblate spheroids of larger size, the extinction spectrum is markedly different for configurations KzEx and KyEx, *i.e.* same electric field polarization, but different incident direction. In particular, the quadrupolar LSP resonance (and even higher order) is particularly pronounced in the KyEx case (see 2(a)). This can be easily understood since retardation effects should be larger in this case where $\boldsymbol{k}$ is along one of the long axis of the particle. Moreover, this quadrupolar LSP resonance also redshifts and broadens as the size increases (see Fig. 2a and Fig. 3). Note however that the dipolar LSP resonance remains almost identical for both KzEx and KyEx configurations.

Finally, we note that the results obtained for $r_0 = 10$ nm are close to those of the ES approximation. However, it is clear from Fig. 2 and 3 that the ES approximation fails spectacularly for larger sizes, as seen in the large resonance shifts observed already for $r_0 = 30$ nm, for which particle dimension along the short axis is nevertheless still small (see Table 1).

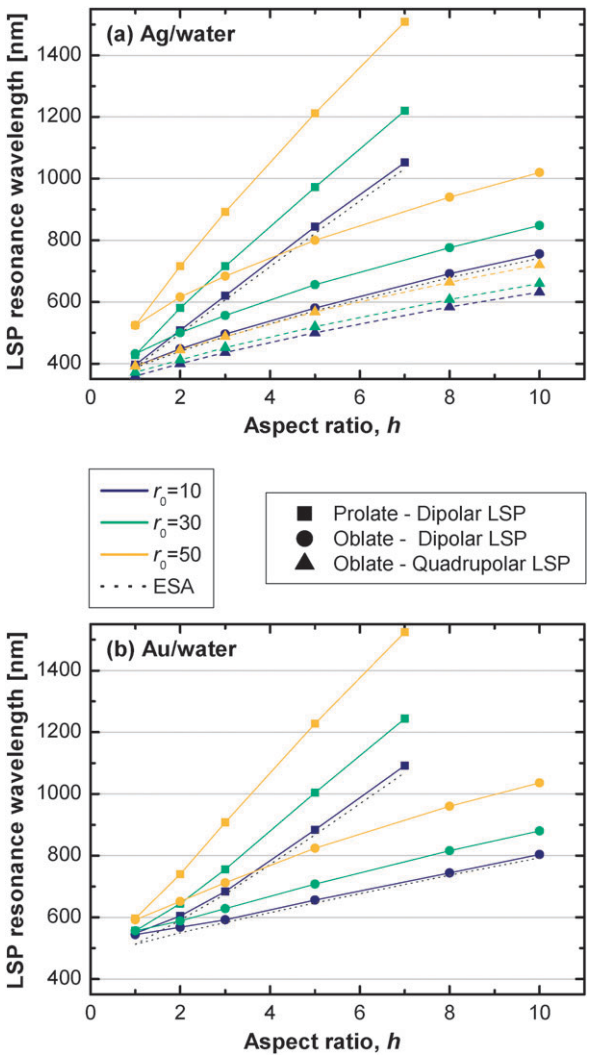

Fig. 3 Predicted LSP resonances as a function of aspect ratio for (a) silver and (b) gold oblate and prolate spheroids of various sizes embedded in water.

IV. Average local field enhancements

Let us now focus on the local field enhancements, starting with the *average* SERS EFs, $\langle F \rangle$. Their wavelength dependence is shown in Fig. 4 for the same representative cases as those studied earlier in Fig. 2.

As before, some of the features evident in Fig. 4 are qualitatively expected from earlier studies of either the spheroids in the ESA or the sphere within Mie theory, in particular: (i) The wavelength dependence of the average SERS EF exhibits the same dependence as those of the (far-field) extinction spectra (shown in Fig. 2). Note however that the magnitude of the average SERS EF at resonance cannot be inferred from the far-field spectra. In fact, the extinction coefficients at resonance are always of the same order (between 10 and 50), while average SERS EFs at resonance vary by several orders of magnitude (10^2–10^8) depending on the case. The values of the average SERS EFs at the most important resonances (dipolar and quadrupolar LSP resonances) are summarized in Fig. 5 as a function of size and aspect ratio. (ii) Average SERS EFs increase as the aspect ratio increases, and are larger for prolate spheroids compared to oblate spheroids (which are less "pointy"). This is also predicted qualitatively by the ESA.[1] (iii) Average SERS EFs decrease as the size increases, as predicted by Mie theory in the simple case of a sphere.[1]

However, only a quantitative study, *i.e.* exact 3D electrodynamic calculations as presented here, can ascertain to which degree the size-induced decrease in $\langle F \rangle$ may be compensated by a larger aspect ratio. This is an important point since controlled fabrication of ultra-small metallic particles of elongated shape remains an experimental challenge. In fact, most experiments on elongated particles have used relatively large particles, with r_0 = 30–50 nm. As an example of this trade-off for a silver prolate spheroid, a particle with r_0 = 10 nm and h = 2 has the same average SERS EF ($\approx 10^6$) at resonance as one with r_0 = 30 nm and $h \approx 4$ or one with r_0 = 50 nm and $h \approx 7$. Note that the actual resonance is at a different wavelength in each case (see Fig. 3). Other similar examples can be easily inferred from Fig. 5.

A couple of additional features of our results are worth pointing out: (i) Reasonably large average SERS EFs ($\sim 10^6$) (and maximum EFs in excess of $\sim 10^8$ as will be shown) can be obtained even on relatively large objects, as for example in the case of a prolate spheroid of volume-equivalent radius of r_0 = 50 nm with an aspect ratio of h = 7. The full encapsulating dimensions of such a particle are around 350 × 50 nm. Such large average and maximum SERS EFs would not have been expected *a priori* for such a large particle because of radiation damping. (ii) As for the far-field properties, the quadrupolar LSP resonance is particularly prominent for large oblate particles in the KyEx excitation configuration (see Fig. 4a). In fact, the average SERS EF can be larger at the quadrupolar LSP resonance than at the dipolar LSP resonance, as for example for r_0 = 50 nm, h = 8. Such a feature is entirely missed in the ES approximation or its generalization. The excitation of this quadrupolar LSP resonance is more explicitly visible in the actual distribution of enhancement factors (punctual here, not average) on the surface as shown in Fig. 6. For the same oblate spheroid (Ag/water with h = 3 and r_0 = 50 nm) at the quadrupolar LSP wavelength (λ = 488 nm) and with the same incident field polarization

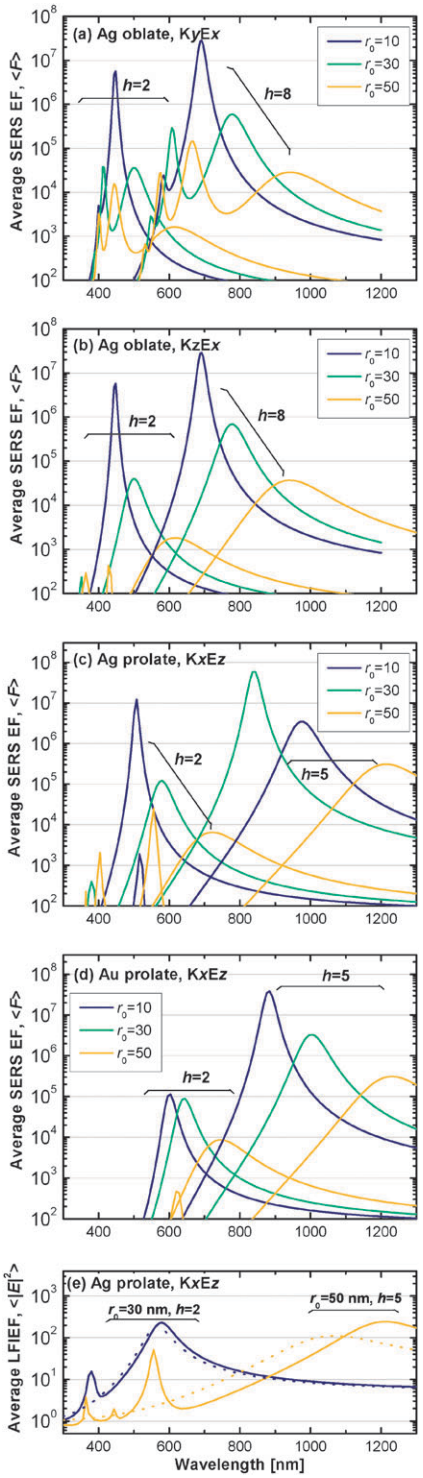

Fig. 4 Predicted spectral dependence of the surface-averaged SERS EF at zero Stokes shift in the $|E|^4$-approximation, $\langle F \rangle$, for the same cases as in Fig. 2. Section (e) shows a comparison of the T-matrix predictions for the average LFIEF ($\langle |E|^2/|E_0|^2 \rangle$) with those of the modified ES approximation as presented in ref. 13 in two representative cases.

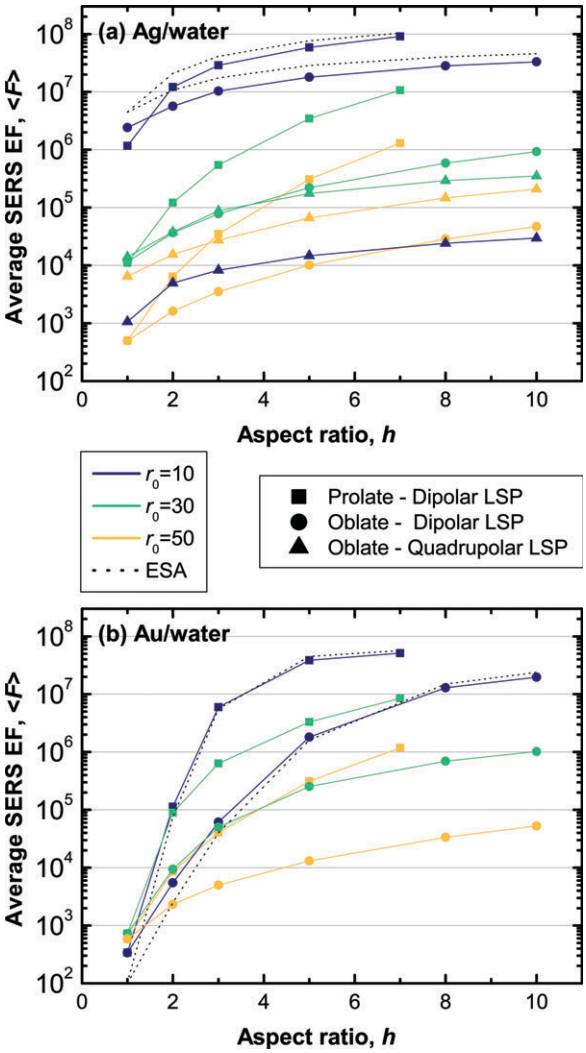

Fig. 5 Predicted average SERS EFs at the LSP resonance wavelength as a function of aspect ratio for (a) silver and (b) gold oblate and prolate spheroids of various sizes embedded in water.

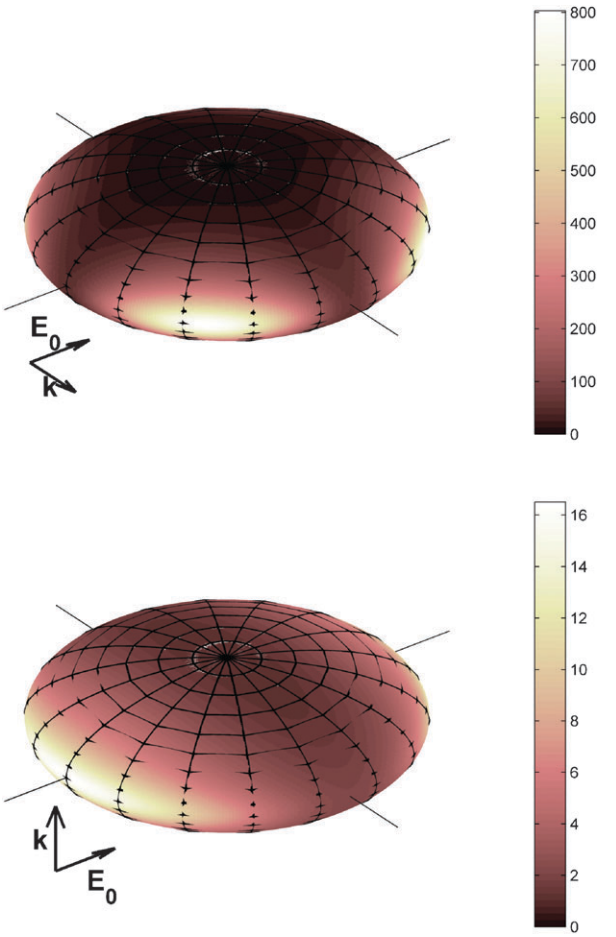

Fig. 6 Distribution of the local field intensity EF on the surface ($M \approx \sqrt{F}$) for a silver oblate spheroid ($h = 3$, $r_0 = 50$ nm) in water, for excitation at 488 nm (*i.e.* the quadrupolar LSP resonance) with electric field polarization along x and incidence along either y (KyEx configuration—top) or z (KzEx configuration—bottom). The quadrupolar resonance is clearly excited in the first case, but not in the second. The ES approximation predicts the same dipolar response in both cases.

(along x), the quadrupolar character of the resonance is clearly visible for incidence along the long axis (KyEx), while a dipolar response is obtained for incidence along the short axis (KzEx). The ES approximation would predict the same dipolar response in both configurations. (iii) It is also worth emphasizing that the average SERS EFs for silver and gold particles become comparable at large redshift, *i.e.* large size and/or aspect ratio (see Fig. 4c–d). This is not so surprising since their optical properties become increasingly similar in the near infrared region. This aspect has been extensively emphasized and discussed in ref. 1.

Finally, as shown explicitly in Fig. 4e, it is clear that even the inclusion of dynamic depolarization and radiative corrections in the ESA[13] is insufficient to provide quantitative predictions in agreement with the exact T-matrix solution in terms of (i) the red-shift of the resonance, (ii) the magnitude of the enhancements, and more spectacularly perhaps (iii) the importance of higher order resonances. This is particularly evident for the case $r_0 = 50$ nm, $h = 5$, and it is even visible for relatively small sizes and small aspect ratio (for example $r_0 = 30$ nm, $h = 2$, see Fig. 4e). This justifies the necessity for more accurate calculations as presented here.

V. Maximum local field enhancements and localization

We now complete this study by focusing on the maximum SERS EF, *i.e.* the punctual SERS EF at the point on the particle surface where it is maximum. Maximum SERS EF can be typically several orders of magnitude larger than the average SERS EF,[9] a property that is often exploited for single molecule detection.[8] Such a feature is intrinsically linked to the strong localization of regions of very high local field enhancements, so-called hot-spots.[8,9]

A relatively simple way to quantify both the magnitude of the maximum SERS EF and the degree of localization is to consider the ratio between maximum and average SERS EFs: $R = F_{\max}/\langle F \rangle$. $R = 1$ indicates a perfectly uniform EF on the

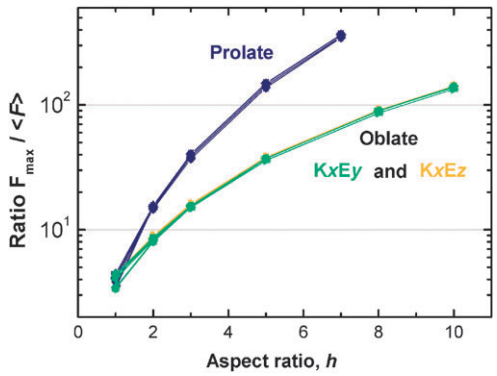

Fig. 7 Aspect ratio dependence of the ratio $F_{max}/\langle F\rangle$, between the maximum SERS EF (at the tip of the spheroid on the axis of the incident polarization) and the surface-averaged SERS EF. These SERS EFs are calculated at the dipolar resonance of the spheroid (*i.e.* at the dipolar resonance wavelengths summarized in Fig. 3). A large number of plots for different cases are superimposed to demonstrate the universality of this dependence: eight cases for prolate spheroids with either r_0 = 10, 30, 50 nm or within the ESA, each for either gold or silver particles in water; sixteen cases for oblate spheroids with either r_0 = 10, 30, 50 nm or within the ESA, each for either gold or silver particles in water, and each for K*y*E*x* and K*z*E*x* configurations. It is clear from these plots that, up to very small variations, this ratio is entirely determined by the shape parameters of the particle: type (prolate and oblate) and aspect ratio. It is almost independent of material (Ag or Au), size, and resonance wavelength.

surface. Moreover, the larger R, the stronger the localization. R reaching up to 250–500 are for example predicted for hot-spots formed at the junction between two-closely spaced metallic nanospheres with a separation of $\approx$2 nm.[9]

We restrict ourselves in the following to the values at the main dipolar resonance (whose wavelengths λ_{Res} are summarized in Fig. 3 for the systems under study). This is typically where F_{max} and F are the largest. Moreover, the maximum SERS EF then occurs at the two points at the "tip" of the spheroid along the axis of the incident field polarization (as predicted also in the ES approximation). Fig. 7 shows the aspect-ratio-dependence of $R(\lambda_{res})$ for spheroids in most of the cases studied so far: Ag and Au particles in water, prolate or oblate in both K*y*E*x* and K*z*E*x* configurations, sizes of r_0 = 10, 30, or 50 nm or within the ES approximation, and any combinations thereof. It is remarkable that for all these cases, the plot $R(\lambda_{Res})$ falls almost exactly on one of two lines: one for prolate and one for oblate spheroids (see Fig. 7). It is clear from these plots that $R(\lambda_{res})$, and therefore the degree of localization at the hot-spot is independent of material (Ag or Au) and size (and is therefore not affected by radiation or retardation effects). It is in fact an intrinsic property of the *particle shape*, characterized here by its type (oblate or prolate) and aspect ratio. This property can in fact be traced back to the strongly dipolar nature of the resonance: the magnitude of the induced dipole is affected by all parameters (material, size, shape, *etc*...). However, the position dependence of the field it creates on the particle surface is determined only by geometrical factors. Nevertheless, such a remarkable universality would certainly deserve further investigations, in particular to assess whether it can be generalized to any particle shapes. A direct consequence of this observation is that the magnitude of the maximum SERS EF follow the same qualitative size dependence as the average SERS EF, the most salient features of which have been discussed in the previous section. The shape-dependence can also be inferred from the convolution of the results in Fig. 5 and 7. In particular, the increased localization at large aspect ratios result in even larger shape-induced increases in F_{max} than those observed for F. This is a manifestation of the "lightning rod effect" and is also qualitatively predicted in the ES approximation.[1] As a result, although maximum SERS EF decrease markedly as the size increases, this may be more easily compensated by an increase in aspect ratio. In the case of a silver or gold prolate spheroid of aspect ratio h = 7, maximum SERS EFs of the order of 2–4 $\times$ 10^{10} are achieved for small sizes (r_0 = 10 nm), and remain reasonably large, of the order of 4 $\times$ 10^8 for the largest size of r_0 = 50 nm. Finally, we also note that $R(\lambda_{res})$ reaches a value of the order of $\sim$370 for prolate particles of aspect ratio h = 7. This is comparable with what is obtained at junctions between particles. Both large field enhancement localization and large punctual SERS EF, in short SERS hot-spots, can therefore be induced by shape effects, even at relatively large sizes. Such elongated particles provide another class of hot-spot-containing SERS substrates, in addition to the standard example of closely-spaced particles.

VI. Conclusion

We have presented an in-depth study of the EM properties of metallic spheroids, covering a large parameter space of interest to SERS. The results do not rely on any type of approximation, numerical or otherwise (*e.g.* electrostatics) and confirm many aspects of the accepted phenomenological description of size and shape effects: (i) larger sizes lead to red-shifted, broadened LSP resonances with less local field enhancements (ii) large aspect ratio lead to a red-shifted LSP resonance (for polarization along long axis) with increased local field enhancements. In addition, this study provides a *quantitative* estimation of how these effects eventually contribute to the shape-and-size dependence of both average and maximum SERS EFs. Finally, these calculations have highlighted a couple of new effects: (i) the importance of quadrupolar resonances in oblate spheroids of intermediate of large size, which may result in a larger average SERS EF than the dipolar resonance. (ii) the fact that the degree of field-enhancement localization (at a hot-spot) at resonance is determined only by shape parameters and is independent of size and material parameters.

Acknowledgements

This work was supported by a Victoria University Science Faculty strategic research grant for summer research assistant.

References

1 E. C. Le Ru and P. G. Etchegoin, *Principles of Surface-Enhanced Raman Spectroscopy and Related Plasmonic Effects*, Elsevier, Amsterdam, 2009.

2 R. Aroca, *Surface-Enhanced Vibrational Spectroscopy*, John Wiley & Sons, Chichester, 2006.
3 G. A. Baker and D. S. Moore, *Anal. Bioanal. Chem.*, 2005, **382**, 1751–1770.
4 D. A. Stuart, J. M. Yuen, N. Shah, O. Lyandres, C. R. Yonzon, M. R. Glucksberg, J. T. Walsh and R. P. V. Duyne, *Anal. Chem.*, 2006, **78**, 7211.
5 A. Barhoumi, D. Zhang, F. Tam and N. J. Halas, *J. Am. Chem. Soc.*, 2008, **130**, 5523–5524.
6 E. C. Le Ru, M. Meyer and P. G. Etchegoin, *J. Phys. Chem. B*, 2006, **110**(4), 1944–1948.
7 E. C. Le Ru, E. Blackie, M. Meyer and P. G. Etchegoin, *J. Phys. Chem. C*, 2007, **111**(37), 13794–13803.
8 P. G. Etchegoin and E. C. Le Ru, *Phys. Chem. Chem. Phys.*, 2008, **10**, 6079–6089.
9 E. C. Le Ru, P. G. Etchegoin and M. Meyer, *J. Chem. Phys.*, 2006, **125**, 204701–204714.
10 J. B. Jackson, S. L. Westcott, L. R. Hirsch, J. L. West and N. J. Halas, *Appl. Phys. Lett.*, 2003, **82**, 257–259.
11 E. Prodan, P. Nordlander and N. J. Halas, *Nano Lett.*, 2003, **3**, 1411–1415.
12 A. Wokaun, *Solid State Phys.*, 1984, **38**, 223–293.
13 E. J. Zeman and G. C. Schatz, *J. Phys. Chem.*, 1987, **91**, 634–643.
14 K. L. Kelly, E. Coronado, L. L. Zhao and G. C. Schatz, *J. Phys. Chem. B*, 2003, **107**, 668–677.
15 M. Kerker, D.-S. Wang and H. Chew, *Appl. Opt.*, 1980, **19**(24), 4159–4174.
16 B. J. Messinger, K. U. von Raben, R. K. Chang and P. W. Barber, *Phys. Rev. B*, 1981, **24**, 649.
17 A. Wokaun, J. P. Gordon and P. F. Liao, *Phys. Rev. Lett.*, 1982, **48**(14), 957–960.
18 M. Meier and A. Wokaun, *Opt. Lett.*, 1983, **8**(11), 581–583.
19 J. Jin, *The Finite Element Method in Electromagnetics*, Wiley-IEEE Press, New York, 2nd edn, 2002.
20 A. Taflove and S. Hagness, *Computational Electrodynamics: the Finite-Difference Time-Domain Method*, Artech House, Boston, 2000.
21 U. Hohenester and J. Krenn, *Phys. Rev. B*, 2005, **72**, 195429-1–9.
22 E. M. Purcell and C. R. Pennypacker, *Astrophys. J.*, 1973, **186**, 705–714.
23 W.-H. Yang, G. C. Schatz and R. P. V. Duyne, *J. Chem. Phys.*, 1995, **103**(3), 869–875.
24 S. Asano and G. Yamamoto, *Appl. Opt.*, 1975, **14**(1), 29–49.
25 S. Asano and G. Yamamoto, *Appl. Opt.*, 1979, **18**, 712.
26 P. C. Waterman, *J. Opt. Soc. Am.*, 1969, **45**, 1417–1429.
27 P. C. Waterman, *Phys. Rev. D*, 1971, **3**, 825–839.
28 P. W. Barber and C. Yeh, *Appl. Opt.*, 1975, **14**, 2864–2872.
29 P. C. Waterman, *J. Appl. Phys.*, 1979, **50**, 4550.
30 M. I. Mishchenko, L. D. Travis and A. A. Lacis, *Scattering, Absorption and Emission of Light by Small Particles*, Cambridge University Press, Cambridge, 3rd electronic release edn, 2002.
31 M. I. Mishchenko, G. Videen, V. A. Babenko, N. G. Khlebtsov and T. Wriedt, *J. Quantum Spectrosc. Radiat. Transfer*, 2004, **88**, 357–406.
32 M. I. Mishchenko, G. Videen, V. A. Babenko, N. G. Khlebtsov and T. Wriedt, *J. Quantum Spectrosc. Radiat. Transfer*, 2007, **106**, 304–324.
33 M. I. Mishchenko, G. Videen, N. G. Khlebtsov, T. Wriedt and N. T. Zakharova, *J. Quantum Spectrosc. Radiat. Transfer*, 2008, **109**, 1447–1460.
34 B. N. Khlebtsov and N. G. Khlebtsov, *J. Phys. Chem. C*, 2007, **111**, 11516–11527.
35 P. W. Barber, R. K. Chang and H. Massoudi, *Phys. Rev. Lett.*, 1983, **50**, 997–1000.
36 P. W. Barber, R. K. Chang and H. Massoudi, *Phys. Rev. B*, 1983, **27**, 7251–7261.
37 P. G. Etchegoin, E. C. Le Ru and M. Meyer, *J. Chem. Phys.*, 2006, **125**(16), 164705–1–3.
38 P. W. Barber and S. C. Hill, *Light Scattering by Particles: Computational Methods*, World Scientific, Singapore, 1990.
39 E. C. Le Ru and P. G. Etchegoin, *Chem. Phys. Lett.*, 2006, **423**, 63–66.
40 J. Zuloaga, E. Prodan and P. Nordlander, *Nano Lett.*, 2009, **9**(2), 887–891.